Agricultural Systems 238 (2026) 104848

Contents lists available at ScienceDirect

Agricultural Systems

journal homepage: www.elsevier.com/locate/agsy

Research Paper

# Causal inference reveals the dominant role of climate-adaptation coupling in future potato production

Zhihao He [a,b], Tengcong Jiang [a,b], Lin Zhu [c], Ning Yao [d,e], Yi Li [e], Hao Feng [a,b,f], De Li Liu [g], Liang He [h], Jianqiang He [d,e,f,*], Qiang Yu [a,b,**]

[a] State Key Laboratory of Soil and Water Conservation and Desertification Control, Institute of Soil and Water Conservation, Northwest A&F University, Yangling 712100, China
[b] College of Soil and Water Conservation Science and Engineering, Northwest A&F University, Yangling 712100, Shaanxi, China
[c] College of Natural Resources and Environment, Northwest A&F University, Yangling 712100, Shaanxi, China
[d] Key Laboratory for Agricultural Soil and Water Engineering in Arid Area of Ministry of Education, Northwest A&F University, Yangling 712100, China
[e] College of Water Resources and Architectural Engineering, Northwest A&F University, Yangling 712100, Shaanxi, China
[f] Institute of Water-Saving Agriculture in Arid Areas of China, Northwest A&F University, Yangling 712100, Shaanxi, China
[g] NSW Department of Primary Industries, Wagga Wagga Agricultural Institute, Wagga Wagga, NSW 2650, Australia
[h] National Meteorological Center, Beijing 100081, China

## HIGHLIGHTS

- Early planting, rainfed, increased nitrogen and mulching increases potato yields by 19–21% in future.
- The causal benefits of adaptation weaken under the SSP585 and in the long-term future.
- Future adaptation should prioritize heat stress mitigation over water dependence for potato.
- Climate-adaptation couplings dominate future yield variability, accounting for 37.6–42.4% of potato yield changes.

## GRAPHICAL ABSTRACT

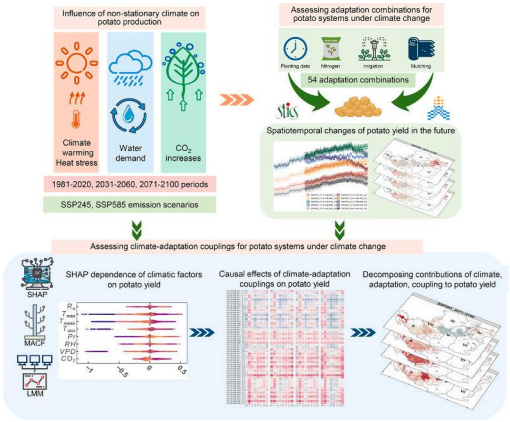


## ARTICLE INFO

Editor: Krishna Devkota

*Keywords:*
Potato

## ABSTRACT

*CONTEXT:* Climate change is transforming agricultural production at an unprecedented pace and poses a substantial threat to food security. Although many adaptation measures have been proposed, the causal effects of climate-adaptation couplings to potato yield remain poorly understood. In the climate-sensitive potato

* Correspondence author at: Key Laboratory for Agricultural Soil and Water Engineering in Arid Area of Ministry of Education, Northwest A&F University, Yangling 712100, China.
** Correspondence author at: State Key Laboratory of Soil and Water Conservation and Desertification Control, Institute of Soil and Water Conservation, Northwest A&F University, Yangling 712100, China.
*E-mail addresses:* jianqiang_he@nwafu.edu.cn (J. He), yuq@nwafu.edu.cn (Q. Yu).

https://doi.org/10.1016/j.agsy.2026.104848
Received 29 January 2026; Received in revised form 29 May 2026; Accepted 31 May 2026
Available online 6 June 2026

Climate-adaptation couplings
Causal inference
Yield sensitivity

production region of Loess Plateau in China, clarifying this coupling process is critical for developing effective adaptive production strategies.

*OBJECTIVE:* This study aims to evaluate the impacts of different adaptation packages on potato yield under future non-stationary climate conditions on the Loess Plateau of China, and to clarify the role of climate-adaptation coupling in yield formation using causal inference.

*METHODS:* We integrated multi-model simulations, interpretable machine learning, and a multi-arm causal forest model to systematically assess the impacts of 54 adaptation combinations on future potato yield under the SSP245 and SSP585 scenarios. Standardized mixed-effects models were used to decompose the contributions of climatic factors, adaptation measures, and their coupling effects to yield variation.

RESULTS AND CONCLUSIONS

We find that the combination of early planting, rainfed management, increased nitrogen application, and plastic film mulching was the highest-yielding strategy, increasing projected yields by 19.50-20.94% in future. However, adaptation benefits decline over time and with higher emission intensity, especially during 2071-2100 under SSP585. Causal analysis within the simulated framework shows that the treatment effects of most adaptation combinations are diminished by climate-adaptation coupling. Meanwhile, heat stress progressively offsets the positive influences of water and $CO_2$ fertilization. Using standardized mixed-effects models, we quantify that climate-adaptation coupling explains 37.63-42.42% of yield variation, significantly higher than the effect of single climatic or adaptation factors. The optimal adaptation strengthens positive couplings such as nitrogen-precipitation and mulching-precipitation, improving water-nutrient synergy under rainfed conditions while avoiding the compounded hot-wet stress that can arise from irrigation combined with mulching under high temperatures. Spatially, the arid, cool western plateau benefits most from couplings, although that advantage is reduced under SSP585.

*SIGNIFICANCE:* This study demonstrates that sustaining future potato production requires dynamic, regionally differentiated adaptation pathways that prioritize heat stress mitigation and actively reinforce positive climate-adaptation couplings. These findings provide a mechanistic basis for designing climate-smart potato cropping systems.

## 1. Introduction

Global climate change is reshaping agricultural production at an unprecedented rate and poses a fundamental threat to food security. Observational and modeling studies consistently show that rising temperatures are a key driver of yield declines for major staples: each 1 °C increase can reduce global yields of wheat, maize, rice, and soybean by roughly 3-10% on average (Abramoff et al., 2023; Schlenker and Roberts, 2009; Zhao et al., 2017). Although higher atmospheric $CO_2$ can partly offset warming-induced losses through $CO_2$ fertilization under some conditions (Fitzgerald et al., 2016; Makowski et al., 2020), that benefit depends strongly on water availability and can be overwhelmed by intensifying heat stress under continued warming (Jägermeyr et al., 2021; McDermid et al., 2023). Understanding and quantifying crop production risks under climate change and designing effective adaptation measures are therefore central challenges for securing future food supplies (Challinor et al., 2014).

To address climate risks, multiple field-scale adaptation strategies have been proposed and extensively studied, primarily including adjusting crop varieties and sowing dates, optimizing irrigation and nutrient management, and adopting plastic film mulching. Both modeling and empirical studies indicate that such measures can effectively alleviate climatic stress and help maintain or even enhance crop yields (He et al., 2024; Minoli et al., 2022; Ren et al., 2025). However, the actual effectiveness of these adaptation measures is not independent of the changing climate. Their influence on crop growth operates through both direct and indirect pathways, with the indirect pathways largely mediated by the coupling effects between climate and management on crop development. For example, earlier sowing functions mainly by shifting sensitive crop growth stages away from seasonal high-temperature periods. Meanwhile, irrigation not only directly mitigates water stress but can also reduce heat damage through its evaporative cooling effect (Dobor et al., 2016; Li et al., 2020). Furthermore, studies have shown that increased nitrogen application can enhance the yield response of rice to elevated $CO_2$ concentrations (Kim et al., 2003). While plastic film mulching improves field microclimate and soil moisture conditions, under persistent warming its warming effect may amplify heat stress on potato yield. Specifically, by altering surface albedo and blocking water vapor exchange, mulching increases soil temperature and conserves moisture, but during hot seasons it may also elevate canopy temperature beyond the optimal range, thereby inhibiting tuber formation and bulking (Brisson et al., 2009; Steduto et al., 2009). Currently, understanding of the coupling effects between different adaptation measures and various climatic factors remains notably insufficient. Existing research has yet to systematically reveal the strength, spatiotemporal dynamics, and response characteristics of these couplings under different emission scenarios. Against the backdrop of climate change, traditional statistical methods struggle to effectively control for confounding factors, making it difficult to accurately identify the true causal effect of climate-adaptation coupling on yield. This can lead to the actual effectiveness of adaptations being either overestimated or underestimated (Heinicke et al., 2022). Causal inference methods have recently emerged as powerful tools to disentangle complex relationships in agricultural systems under climate change (Kluger et al., 2022). By explicitly modeling treatment assignments and controlling for confounding factors, these approaches offer more credible estimates of how climate-adaptation interactions affect crop yield. However, their application to regional-scale adaptation assessment remains limited. Therefore, moving from qualitative description to quantitative analysis to thoroughly unravel the mechanisms through which climate-adaptation coupling influences potato yield has become a key focus and challenge in current research.

In China, promoting potato as a staple has become part of national food security policy (Liu et al., 2021). The Loess Plateau is a typical semi-arid region in China, benefiting from ample sunlight and heat that support its role as a major rainfed potato production region (Fu et al., 2017). Precipitation is concentrated between July and September, coinciding with the critical stages of tuber formation and maturation. Consequently, fluctuations in temperature and rainfall strongly influence potato growth, rendering the crop highly sensitive to environmental variability (Raymundo et al., 2018). The region is also particularly vulnerable to climate change. In recent decades, rising temperatures, shifting precipitation patterns, and more frequent extreme events, such as heatwaves and intense rainfall, have intensified pressure on rainfed agricultural systems (Sun et al., 2016). These changes increase heat stress during the growing season and heighten variability in water availability, thereby diminishing the climatic suitability of traditional planting practices. In light of these challenges,

identifying ways to stabilize and enhance potato yields through targeted adaptation has become urgent. Although prior research has examined crop responses to climate change on the Loess Plateau, important knowledge gaps persist. Prior analyses have yet to disentangle the separate and joint influences of these drivers on yield formation, or to map their evolving spatiotemporal patterns. More importantly, the mechanisms through which key climatic factors, adaptation measures, and their interactions collectively influence yield remain insufficiently understood. A clearer understanding of these mechanisms is therefore vital, as it directly informs the design of targeted adaptation strategies and supports the development of climate-resilient potato production systems, ultimately contributing to long-term regional food security.

To address these knowledge gaps, we focus on potato production systems on Loess Plateau of China. Employing an integrated framework that couples multi-model ensemble simulations, interpretable machine learning, and causal inference, this study is designed to: (1) identify which adaptation measures most effectively enhance potato yield under multiple future climate scenarios, and quantify how their benefits evolve over time and with increasing emission intensity; (2) apply causal inference to clarify whether climate-adaptation coupling effects exist and shape potato yield outcomes under non-stationary climate change based on the simulated framework; and (3) systematically decompose the relative contributions of climatic drivers, adaptation measures, and their couplings to future yield variability. The aim of this study is not only to identify the optimal combination of adaptation measures. By integrating multi-crop model simulations, interpretable machine learning, and causal inference, it systematically reveals how climate conditions shape the effectiveness of adaptation measures and quantifies the extent to which climate-adaptation coupling contributes to future yield variation on the Loess Plateau of China. Therefore, by combining qualitative and quantitative analyses, this study provides important scientific insights for the design of climate-adaptive potato cropping systems and for regional adaptation planning under global warming.

## 2. Materials and methods

### 2.1. Data sources and processing

The potato planting area on Loess Plateau of China was delineated at 0.1° × 0.1° resolution using the Spatial Production Allocation Model (SPAM2010) (Yu et al., 2020) and further refined with data from 126 counties that have long-term potato-planting habits (Fig. 1). A county was classified as long-term if potatoes had been grown there continuously for more than 15 years, based on the China Rural Statistical Yearbook (http://www.stats.gov.cn/). To remove very small-area grid cells, we retained the top 90% of grid cells ranked by harvested potato area for analysis. Daily meteorological data for 1981-2020 were obtained from the China Meteorological Forcing Dataset (CMFD2.0; 0.1° × 0.1° resolution). CMFD2.0 combines ERA5 reanalysis from the European Centre for Medium-Range Weather Forecasts (ECMWF) with observations from Chinese weather stations and incorporates radiation and precipitation products generated using AI methods (He Jie et al., 2025). Future climate projections were derived from 27 global climate models (GCMs) from CMIP6, under SSP245 and SSP585 scenarios (Table S1). These two scenarios were selected to represent contrasting future pathways: SSP245 as a medium-forcing scenario and SSP585 as a high-forcing scenario, allowing us to evaluate adaptation effectiveness under different levels of climate stress. Climatic factors used in the analysis included solar radiation ($R_n$, MJ m$^{-2}$), maximum temperature ($T_{max}$, °C), minimum temperature ($T_{min}$, °C), mean temperature ($T_{mean}$, °C),

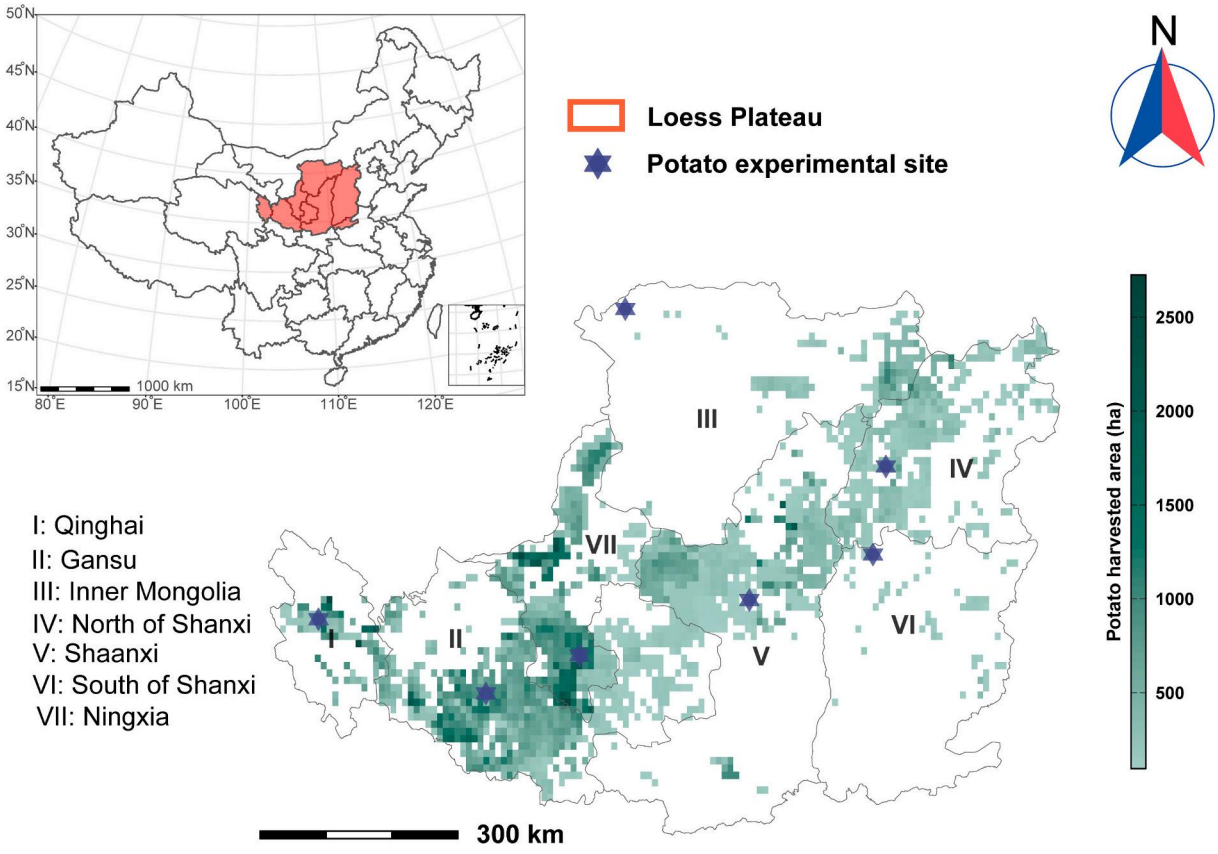


**Fig. 1.** Spatial distribution of potato planting areas on the Loess Plateau (red-shaded region on the map of China). Blue stars indicate the experimental sites for potato. Regions I to VII correspond to Qinghai, Gansu, Inner Mongolia, northern Shanxi, Shaanxi, southern Shanxi, and Ningxia Province of China, respectively. (For interpretation of the references to colour in this figure legend, the reader is referred to the web version of this article.)

precipitation (*Pr*, mm), relative humidity (*RH*, %), vapor pressure deficit (*VPD*, kPa), and atmospheric $CO_2$ concentration (ppm). *VPD* was computed from temperature and relative humidity. Scenario $CO_2$ concentrations for SSP245 and SSP585 were estimated using Eq. 1. Soil inputs came from the China Soil Hydraulic Parameters Dataset (1 km × 1 km) and the Harmonized World Soil Database (1 km × 1 km), and included soil physical properties (e.g., field capacity, saturated water content, hydraulic conductivity), nutrient content (nitrate and ammonium N), bulk density, organic carbon, and pH at multiple depths. All climate and soil layers were resampled to a 0.1° grid using bilinear interpolation for the potato yield simulations and reanalysis.

$$\begin{cases} SSP245_{CO_2} = 62.044 + \dfrac{34.002 - 3.8702 \times y}{0.24423 - 1.1542 \times y^{2.4901}} + 0.028057 \times \left( {}^{y} + \right. \\ 2.6287 \times 10^{-4} \times \left( {}^{y} - 9.2751 \times 10^{-7} \times \left( {}^{y} - 2.2448 \times (y - 2030) \right. \right. \\ SSP585_{CO_2} = 757.44 + \dfrac{84.938 - 1.537 \times y}{2.2011 - 3.8289 \times y^{-0.45242}} + 2.4712 \times 10^{-4} \times \left( {}^{y} + \right. \\ 1.9299 \times 10^{-5} \times \left( {}^{y} + 5.1137 \times 10^{-7} \times \left( {}^{y} \right. \right. \end{cases} \quad (1)$$

where *y* represents different years.

### 2.2. Crop model simulation

Because plastic film mulching is widely used on the Loess Plateau, we selected STICS and AquaCrop for simulation, as both include mulching modules. In STICS, mulching is represented mechanistically by modifying several physical processes at the soil surface: (1) the surface albedo is altered, which affects net radiation; (2) the film acts as a physical barrier that reduces soil evaporation and blocks water vapor exchange; and (3) these changes in energy balance and evaporative fluxes influence both crop and soil temperatures (Brisson et al., 2009). AquaCrop uses an empirical parameterization, approximating mulching via an evaporation-reduction coefficient and a thermal-time compensation term (Steduto et al., 2009). Combining these complementary mechanistic and empirical approaches helped reduce simulation uncertainty. Model parameters were calibrated using regionally representative cultivars from the seven long-term agro-meteorological stations (Fig. 1). For each station, observational data were randomly split into calibration (70%) and validation (30%) subsets. Cultivar parameters were fitted for each region through an iterative optimization procedure using the "*optim()*" and "*lm()*" functions in R 4.5.1, producing a complete parameter set for all cultivars in both models (Table S3-S4). Representative cultivars and their management details are listed in Table S2. Calibration and validation performance are shown in Fig. S1, and the calibrated cultivar parameters for both models are provided in Table S3 and S4. The observational data used for calibration and validation were obtained from the seven agro-meteorological stations across the Loess Plateau, covering the period 2001–2019, and all records were collected under plastic film mulching conditions. Across the seven regions, the mean RRMSE for simulated yield were 8.70% (STICS) and 8.95% (AquaCrop) during calibration, and 8.83% (STICS) and 9.16% (AquaCrop) during validation, with ensemble means of 8.83% and 8.99%, respectively (Table S5). These values indicate acceptable model accuracy for regional scale assessments. Then, using the calibrated models, we simulated potato yield for 54 adaptation combinations from 1981 to 2100 under SSP245 and SSP585. The combinations comprised four management factors: planting date (P, P1-P3), irrigation (I, I1-I3), nitrogen rate (N, N1-N3), and mulching (M, M1-M2). And they were grouped by the number of practices adjusted: CK (control, no change), G1 (one practice adjusted), G2 (two), G3 (three), and G4 (all four) (Table S7).

For each sub-region, the area-weighted potato yield ($Y_r^{p,s}$) was calculated using the harvested potato area of each grid cell as the weight:

$$Y_r^{p,s} = \frac{\sum_{i=1}^{m} Y_{grid}^{p,s} \times Area_{grid_i}}{\sum_{i=1}^{m} Area_{grid_i}} \quad (2)$$

where, *i* denotes the number of grid cells within each region, $Y_{grid}^{p,s}$ is the potato yield (t ha$^{-1}$) at the *i*-th grid cell for period *p* under scenario *s*, and $Area_{grid_i}$ is the harvested potato area (ha) of the *i*-th grid cell.

Additionally, to quantitatively characterize the changes in potato yield and climatic factors in future periods, we used the relative change rates between the future and historical periods to represent their rates of change, as expressed in the following formula:

$$\begin{cases} [Yc]_{2031}^{future^{r,s}} = \dfrac{\overline{[Y]_{2031}^{future}}^{r,s} - \overline{[Y]_{1981}^{2020}}^{r}}{\overline{[Y]_{1981}^{2020}}^{r}} \times 100\% \\ [Clc]_{2031}^{future^{r,s}} = \dfrac{\overline{[Cl]_{2031}^{future}}^{r,s} - \overline{[Cl]_{1981}^{2020}}^{r}}{\overline{[Cl]_{1981}^{2020}}^{r}} \times 100\% Cl = \{Rn, Pr, RH, VPD\} \\ [Clc]_{2031}^{future^{r,s}} = \overline{[Cl]_{2031}^{future}}^{r,s} - \overline{[Cl]_{1981}^{2020}}^{r} Cl = \{Tmax, Tmin, Tmean, CO2\} \end{cases} \quad (3)$$

where, $\overline{[Y]_{1981}^{2020}}^{r}$, $\overline{[Y]_{2031}^{future}}^{r,s}$, $\overline{[Cl]_{1981}^{2020}}^{r}$ and $\overline{[Cl]_{2031}^{future}}^{r,s}$ represent the mean values of potato yield (or climatic factors) for region *r* under scenario *s* during the periods 1981-2020, 2031-2060, and 2071-2100, respectively.

### 2.3. Causal effect assessment

The analytical framework integrates several complementary methods with distinct purposes. Random forest and SHAP (Shapley Additive Explanations) analyses serve a descriptive and exploratory role, identifying key climatic drivers and their nonlinear associations with yield. GAMs (Generalized Additive Models) further visualize these nonlinear dependencies. The multi-arm causal forest (MACF) is then employed to estimate causal effects (ATEs) of adaptation measures under different climate conditions within the modeling framework. Finally, linear mixed models (LMMs) are used to decompose yield variation into contributions from climatic factors, adaptation measures, and their interactions, providing a quantitative partitioning of explanatory factors. In short, the SHAP and random forest analyses first describe how individual climatic factors affect yield, providing the background for understanding climate-adaptation coupling. Building on this, the MACF estimates how the causal effects of adaptation measures change with climate conditions, which directly captures the coupling. The LMMs then quantify the contribution of this coupling to yield variation.

Key climatic drivers were first identified using Random Forest regression (Breiman, 2001). Gridded yield was the dependent variable, and growing-season climatic factors were predictors. Models were trained separately for each period, emission scenario, and region using the "*randomForest*" package in R 4.5.1, with optimal hyperparameters determined by 5-fold cross-validation (Supplementary Text 2). Predictor importance was quantified as the percentage increase in mean squared error (%IncMSE). To interpret nonlinear contributions of individual drivers, we applied the SHAP (Eq. S3) framework to compute SHAP values and examined their distributions. We also computed SHAP Value Differences (SVD) between future and historical periods. SVD provides a descriptive measure of how the relative importance of each climatic factor within the random forest model changes over time (Eq. 4). Furthermore, we used GAMs to examine the dependence between key climatic factors influencing potato yield and their corresponding SHAP values. For each climatic variable, the SHAP value was treated as the response variable, and the observed value of that factor served as the dependent variable. Smooth functions in the GAM framework were applied to capture potential nonlinear patterns. This approach enables

both visualization and quantification of how the influence of each climatic factor on yield changes with its magnitude (Eq. 5).

To quantify the contribution of different climatic factors to the rebound of potato yield across various regions of the Loess Plateau during the periods 2031-2060 and 2071-2100 under the SSP245 and SSP585 scenarios, we calculated the SHAP Value Differences (SVD) for each climatic feature relative to the historical baseline period (1981-2020). The calculation formula is as follows:

$$\begin{cases} [SVD^{r,s}]_{2031}^{2060} = \dfrac{\left([\phi^{r,s}]_{2031}^{2060} - [\phi^{r}]_{1981}^{2020}\right)}{[\phi^{r}]_{1981}^{2020}} \times 100\% \\ [SVD^{r,s}]_{2071}^{2100} = \dfrac{\left([\phi^{r,s}]_{2071}^{2100} - [\phi^{r}]_{1981}^{2020}\right)}{[\phi^{r}]_{1981}^{2020}} \times 100\% \end{cases} \tag{4}$$

where, $[\phi^{r}]_{1981}^{2020}$, $[\phi^{r,s}]_{2031}^{2060}$ and $[\phi^{r,s}]_{2071}^{2100}$ denote the SHAP values of a given climatic factor for region r under scenario s during the periods 1981-2020, 2031-2060, and 2071-2100, respectively.

Additionally, we employed Generalized Additive Models (GAMs) to analyze the nonlinear dependencies between individual climatic factors and their corresponding SHAP values. The model is specified as follows:

$$\begin{cases} g(E[SHAP|X]) = \beta 0 + \sum_j f_j(X_j) \\ f_j(X_j) = \sum_{k=1}^{K_j} \beta_{jk} b_{jk}(X_j) \end{cases} \tag{5}$$

where $X_j$ represents an individual climatic factor. The smooth term $f_j(X_j)$ is fitted using a spline smoothing function, with a penalty applied to control smoothness and prevent overfitting. We employed the R package *"mgcv"* to automatically optimize the smoothing parameter $f_j(X_j)$ for each climatic factor. $b_{jk}(X_j)$ denotes the set of basic functions used for the $j$-th climatic factor, which specified as thin-plate spline bases; $\beta_{jk}$ refers to the corresponding coefficients to be estimated; and $K_j$ indicates the number of basic functions, which was set to 4 in this analysis.

The causal effects of adaptation measures were estimated as ATE using a MACF implemented in the "*grf*" package. MACF combines propensity-score estimation, honest tree building, adaptive partitioning, ensemble variance reduction, and asymptotic inference to produce unbiased, consistent treatment-effect estimates in high-dimensional settings (Eq. 6). All importance metrics and ATEs (with 95% confidence intervals) were obtained from 1000 bootstrap samples. We examined the distribution of ATEs across different adaptation and climatic factors to assess potential diminishing marginal returns as the number of measures increased.

$$\begin{cases} \hat{\tau}(x) = \underset{\tau}{argmin} \sum_{i=1}^{n} a_i(x)(Y_i - \hat{m}^{(-i)}(X_i) - c(x) - \langle W_i - \hat{e}^{(-i)}(X_i)\, \tau(X_i) \rangle)^2 \\ \widehat{ATE}_k = \dfrac{1}{N} \sum_{i=1}^{n} \hat{\tau}_k(X_i), k = 1, \ldots, K-1 \end{cases} \tag{6}$$

where $\hat{\tau}(x)$ denotes the vector of Conditional Average Treatment Effects (CATE) estimated by the MACF by minimizing the weighted sum of squared residuals. $a_i(x)$ is the weighting function produced by the generalized random forest, reflecting the "proximity" or influence weight of training sample $i$ on the target point $x$. $Y_i$ represents the standardized potato yield for the $i$-th observational unit. $\hat{m}^{(-i)}(X_i)$ is the estimate of $m(X) = E[Y|X]$, capturing the baseline effect of covariates on the outcome. $X_i$ is the covariate vector for the $i$-th observational unit, describing the climatic factors that influence potato yield. $c(x)$ is the local intercept at the target point $x$, absorbing constant offsets that are independent of the treatment effect. $W_i$ denotes the treatment assignment vector for sample $i$, indicating the combination of adaptation measures applied (excluding the control CK). $\hat{e}^{(-i)}(X_i)$ is the vector estimate of the conditional expectation $e(X) = E[W|X]$. $\tau(X_i)$ denotes the conditional treatment-effect vector. $\widehat{ATE}_k$ is the sample-average CATE for the $k$-th treatment arm ($k$ = 1, …, K-1, relative to CK), with 95% confidence intervals derived from 1000 bootstrap replications.

In the MACF framework, the 54 adaptation combinations (including the control) were treated as multi-valued treatments ($W$), and the climatic factors were included as covariates ($X$). The model estimates the conditional average treatment effect (CATE) for each adaptation combination relative to the control, given the observed climate conditions. Consequently, the climate-adaptation coupling effect is captured by the variation in ATE across different climate spaces: if the ATE of a given adaptation combination changes substantially under different climatic conditions, this indicates the presence and magnitude of a climate-adaptation coupling effect. In addition, the ATE estimated here represents the expected yield difference between a given adaptation combination and the control under the specified climate conditions, as evaluated within the crop modeling framework.

### 2.4. Yield sensitivity and factor-contribution decomposition

To quantify the effects of climatic drivers, adaptation measures, and their coupling effects on yield, we fitted standardized linear mixed-effects models (LMMs) for each region using the "*lme4*" package (Eq. 7). The standardized gridded yield was the response. Fixed effects comprised three sets of predictors: climatic factors, adaptation measures, and their two-way coupling. Year and grid cell were included as random effects to account for unobserved temporal and spatial heterogeneity. Climatic variables and yield were standardized; adaptation measures were treated as ordered categorical fixed effects (low to high intensity), yielding dimensionless sensitivity coefficients. To ensure robustness and avoid overfitting, models were fitted independently by region with 1000 bootstrap replicates. For each replicate, the model was refitted and fixed-effect coefficients extracted; the mean coefficient provided the sensitivity estimate and the 5$^{th}$–95$^{th}$ percentile range provided the 95% confidence interval. Significance was annotated at $P < 0.05$, 0.01, and 0.001. Variance inflation factors (VIFs) were computed for all fixed effects in each regional model to assess multicollinearity. The VIF values ranged from 1.7 to 2.2, indicating that multicollinearity did not unduly influence the coefficient estimates.

$$\begin{aligned} Y_{i,j}^{r,p,s} = & \beta 0 + \sum_{n=1}^{8} \beta_n^{r,p,s} Cl_{n,i,j}^{r,p,s} + \sum_{n=9}^{12} \beta_n^{r,p,s} Ad_{n,i,j}^{r,p,s} \\ & + \sum_{n=13}^{45} \beta_n^{r,p,s} \left( Cl_{n,i,j}^{r,p,s} \times Ad_{n,i,j}^{r,p,s} \right) + gr,p,s + yr,p,s + \varepsilon r,p,s \end{aligned} \tag{7}$$

Where $Y_{i,j}^{r,p,s}$ denotes the standardized yield of $i$-th grid in $j$-th year based on $r$-region, $p$-th period, and $s$-th emission scenario. $\beta_n^{r,p,s}$ represents the standardized sensitivity of yield to various factors, which include climatic factors $Cl = \{R_n, T_{max}, T_{min}, T_{mean}, Pr, RH, VPD, CO_2\}$, adaptation measures $Ad = \{P, I, N, M\}$, and their coupling effects $Cl_{n,i,j}^{r,p,s} \times Ad_{n,i,j}^{r,p,s}$. $g_{r,p,s}$ and $y_{r,p,s}$ are the random effects for grid cells and years, respectively, included to control for unobserved spatiotemporal heterogeneity. $\varepsilon_{r,p,s}$ is the residual term.

We decomposed the contribution of factor types to yield variation using the standardized sensitivity coefficients. Total contribution was computed as shown in Eq. 8 and aggregated by category (climatic, adaptation, coupling) to assess relative importance. Factors were classified as positive or negative contributors by the sign of their sensitivity, and proportional contributions within these groups were calculated to identify key drivers of yield gain or loss. This framework simultaneously evaluates direct and interactive effects, providing a systematic decomposition of multi-source drivers of future potato yield change.

$$\begin{cases} Con^{r,p,s} = \dfrac{\left(\sum_{n=1}^{8}\beta_n^{r,p,s}\overline{Cl_{n,j}^{r,p,s}} + \sum_{n=9}^{12}\beta_n^{r,p,s}Ad_{n,j}^{r,p,s} + \sum_{n=13}^{45}\beta_n^{r,p,s}\left(\overline{Cl_{n,j}^{r,p,s}} \times Ad_{n,j}^{r,p,s}\right)\right)\sigma Y_j^{r,p,s}}{\overline{Y_j^{r,p,s}}} \\ Con^{r,p,s} = \sum_{k=1}^{m} Con_{k,Ppositive}^{r,p,s} + \sum_{l=1}^{45-m} Con_{l,Negative}^{r,p,s} \end{cases} \times 100\% \quad (8)$$

Where $Con^{r,p,s}$ denotes the contribution rate of all factors, including both climate change and adaptation measures, to potato yield variation. $\sigma Y_j^{r,p,s}$ represents the mean value of climatic variables for *r*-region, *p*-th period, and *s*-th emission scenario. $\sigma Y_j^{r,p,s}$ and $\overline{Y_j^{r,p,s}}$ are the standard deviation and mean of potato yield for *j*-th grid cell, respectively. $\sum_{k=1}^{m} Con_{k,Ppositive}^{r,p,s}$ and $\sum_{l=1}^{45-m} Con_{l,Negative}^{r,p,s}$ indicate the contribution rates of factors with positive and negative effects on yield, determined by the sign of their corresponding sensitivity coefficients.

## 3. Results

### 3.1. Changes in projected fresh potato yields based on different adaptation combinations

After comparing adaptation combinations, we identified

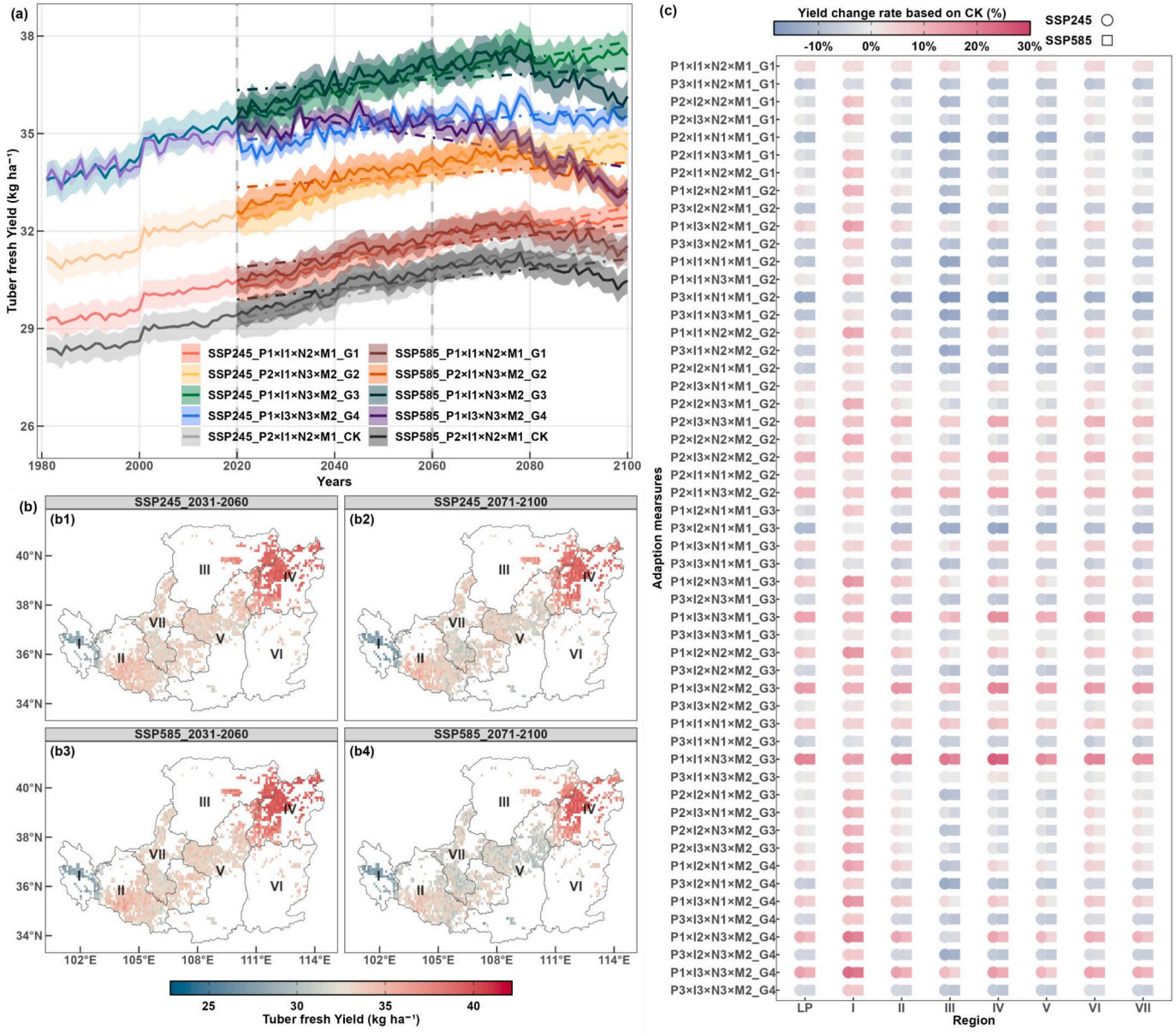


**Fig. 2.** Projected fresh potato yield (hereafter yield) on the Loess Plateau of China under different adaptation combinations, based on the ensemble results of the AquaCrop and STICS models. CK, G1, G2, G3, and G4 represent the control treatment and the adjustment of one, two, three, and four adaptation measures, respectively. (a) Interannual variations in potato yield for the CK group and for the adaptation measures producing the highest and lowest yields within each of the four groups. Shaded areas indicate the 95% confidence intervals, while different colour intensities represent different emission scenarios. The dashed lines denote the fitted linear trends of projected yield in future periods. (b) Spatial distribution of potato yield under the optimal adaptation measures for 2031-2060 and 2071-2100 under SSP245 and SSP585 scenarios. (c) Yield change rates relative to CK for all adaptation combinations during 2071-2100, with different symbols indicating different emission scenarios. The yield change rates for the period 2031-2060 are provided in Fig. S2. Regions I to VII represent Qinghai, Gansu, Inner Mongolia, Northern Shanxi, Shaanxi, Southern Shanxi, and Ningxia, respectively. The same applies to the following figures.

P1×I1×N3×M2 (planting 20 days earlier; rainfed; 1.25 × local nitrogen amount; plastic mulching) as the highest-yielding strategy on the Loess Plateau of China. Compared with the control (CK), this combination significantly increased yield by 19.50%-20.94% in future periods. Notably, P1×I3×N3×M2 was the highest yield combination within Group 4, and the optimal combination increased yield by only 6.26%-6.78%, which was not significant (Table S8). Under SSP245 and SSP585, the highest and lowest group yields rose first and then declined slowly over time (Fig. 2a). In contrast, all climatic factors exhibited a slow increasing trend throughout the century, suggesting that yield changes did not simply follow the direction of climate trends (Fig. S2a). Spatially, highest yields were highest in northern Shanxi (39.92–40.35 t $ha^{-1}$) and lowest in Qinghai (25.06-27.72 t $ha^{-1}$, Fig. 2b). Most combinations showed a southwest-to-northeast increase in yield (Fig. S3-S7), but this pattern weakened under SSP585 in 2071-2100. In particular, the number of combinations that failed to enhance yield was higher under SSP585 than under SSP245. In the 2071-2100 period under SSP585, 24 to 30 combinations no longer improved yield relative to the control, compared with 24 under SSP245 and 21 in the historical period (Fig. 2c and Fig. S8). These results indicate that the potential of adaptation gains for potato yield may decline under future climate change.

Climate change is projected to increase potato yields relative to the 1981-2020 baseline (Eq. S4). Under SSP245, yields across adaptation groups rise by 8.49%-13.75% in 2031-2060 and by 10.57%-17.93% in 2071-2100 (Fig. 3a). Under SSP585, however, the increases are smaller, especially in 2071–2100, when gains reach only 1.05%-12.57%. For the optimal adaptation combination, yield responses show clear spatiotemporal heterogeneity (Fig. 3b). Yields increase markedly in Inner Mongolia, Shanxi, Shaanxi, and Ningxia, particularly in 2031-2060, with gains of 15.54%–20.60% under SSP245 and 16.84%-23.59% under SSP585 (Fig. 3b1, b3). However, by 2071–2100, the yield improvement becomes more limited, especially under SSP585 (Fig. 3b4). Across all 54 adaptation combinations, increasing irrigation produced the largest yield gains for no mulching measures. However, higher irrigation levels led to smaller benefits or even yield declines for mulching measures, which helped compensate for reduced irrigation under future climates (Fig. 3c). Meanwhile, the sharp rise in maximum and minimum temperatures during 2071-2100 may constrain the long-term effectiveness of adaptation measures (Fig. S2b).

### 3.2. Projected causal effects of climatic-adaptation couplings on potato yield

We used random forest models to assess the effects of climatic factors on potato yield across periods and regions. The results show clear spatiotemporal differences in the influence of these factors. During the historical period, $CO_2$ (19.83%) was the most important driver of yield variation, followed by precipitation and temperature variables (Fig. S9). In future periods, mean temperature ($T_{mean}$) became the dominant factor (SSP245: 14.77%, 19.35%; SSP585: 16.04%, 25.41%), with the strongest effects appearing in 2031-2060 and 2071-2100, respectively (Fig. 4a). At the same time, the importance of $CO_2$ and precipitation declined (SSP245: 9.03%, 14.77%; SSP585: 7.17%, 14.07%). Apart from temperature-related factors, the importance of other climatic variables generally declined in the future, indicating that temperature is increasingly becoming a key limiting factor for potato yield on the Loess Plateau.

Regionally, water-related factors (precipitation, *Pr*; relative humidity, *RH*; and *VPD*) played a stronger role than temperature in the semi-arid western region (Qinghai, Gansu, and Ningxia), while the opposite pattern occurred in the east of Loess Plateau (Fig. S9, S10a). The Shapley additive explanations values (SHAP) further revealed contrasting effects of temperature and water. Temperature-related SHAP values increased and then decreased with rising yield, especially under SSP585 scenario (Fig. 4b). The $CO_2$ fertilization effect weakened at higher concentrations in the future, although a slight increase under SSP245 may reflect interactions with warming. Dependence plots also showed distinct relationships between temperature and precipitation-related SHAP values (Fig. S11). By calculating SHAP value differences (SVD) relative to the historical period, we quantified the shift in model-attributed importance of each factor for future yield changes (Fig. S12). The SVD analysis confirms that potato yield will become more sensitive to temperature-related factors, suggesting that future adaptation strategies should prioritize reducing heat stress rather than water limitation.

We then applied causal analysis to evaluate the effects of climatic-adaptation couplings on yield based on the Multi-arm causal forest model (MACF). By calculating the average treatment effect (ATE) relative to scenarios without adaptation, we quantified the extent to which adaptation measures offset or amplify the positive or negative impacts of climate change. Results show that the majority of adaptation combinations produced positive ATEs in both future periods. The proportion of combinations with positive ATE was 70.28% (2031-2060) and 68.63% (2071-2100) under SSP245, and 70.05% and 61.08% under SSP585, respectively (Fig. 5a). This indicates that while adaptation can offset some negative climate impacts, its effectiveness wanes under future conditions. Overall, adaptation outcomes showed strong dependence on emission scenarios. Compared to SSP245, the proportion of positive ATEs under SSP585 was generally lower, especially in the late century period, highlighting the greater challenge of maintaining adaptation benefits under more extreme climate change. Among all adaptation combinations, P1×I1×N3×M2 (the optimal combination) achieved the highest ATE in both periods (SSP245: 2.09, 2.33; SSP585: 2.18, 2.15). Compared to the control (CK), this combination increased yield by approximately 6.58–10.66 t·$ha^{-1}$ through the causal relationship between climate factors and adaptation measures (Fig. 5b).

The ATE of P1×I3×N3×M2 (Group 4) was second only to the optimal combination, with a yield difference of only 0.67 t·$ha^{-1}$ compared to the optimum. However, under SSP585 during 2071-2100, this difference increased to 3.17 t·$ha^{-1}$. This suggests that while the optimal adaptation combination produced a strong and robust positive causal effect under climate change, other combinations showed greater uncertainty across periods and scenarios. Further analysis revealed that although increasing the number of adaptation measures with positive effects could raise the overall ATE, the marginal benefit decreased as more measures were added (Fig. 5c). This underscores the importance of designing efficient and well-balanced adaptation strategies. Regionally, ATE values in Qinghai, Gansu, and Ningxia increased gradually throughout the study period (1981-2100), while other regions showed an initial increase followed by a decline (Fig. S13, S14). Notably, the western Loess Plateau exhibited the highest proportion of positive ATEs under both scenarios (SSP245: 86.83%, 70.76%; SSP585: 82.08%, 72.64%) during 2031-2060 and 2071-2100, respectively. This indicates that causal effects have greater potential to enhance yield in dry and cool regions, likely because the negative impacts of warming are less pronounced in these areas than in the warmer eastern Loess Plateau. In summary, the spatial pattern of causal effects points to the western Loess Plateau as the key area where adaptation measures can achieve the strongest and most stable yield-increasing effects. Conversely, in the warmer and wetter eastern regions, the causal benefits of adaptation are more constrained by intensifying heat stress.

### 3.3. Decompose the contribution of different factors on potato yield

Using standardized linear mixed models across all adaptation combinations, we quantified future potato yield sensitivity to multiple drivers. Precipitation (*Pr*) and $CO_2$ were consistently positive and significant drivers in all periods (Fig. S15, 6). From 2031-2060 to 2071-2100, the sensitivity to *Pr* decreased by 4.40% under SSP245 but increased by 3.43% under SSP585. For $CO_2$, the sensitivity declined by 9.84% under SSP245 but rose by 24.49% under SSP585. Maximum ($T_{max}$) and minimum ($T_{min}$) temperatures emerged as the main stressors among the climatic factors, with stress intensity rising by 13.60% and

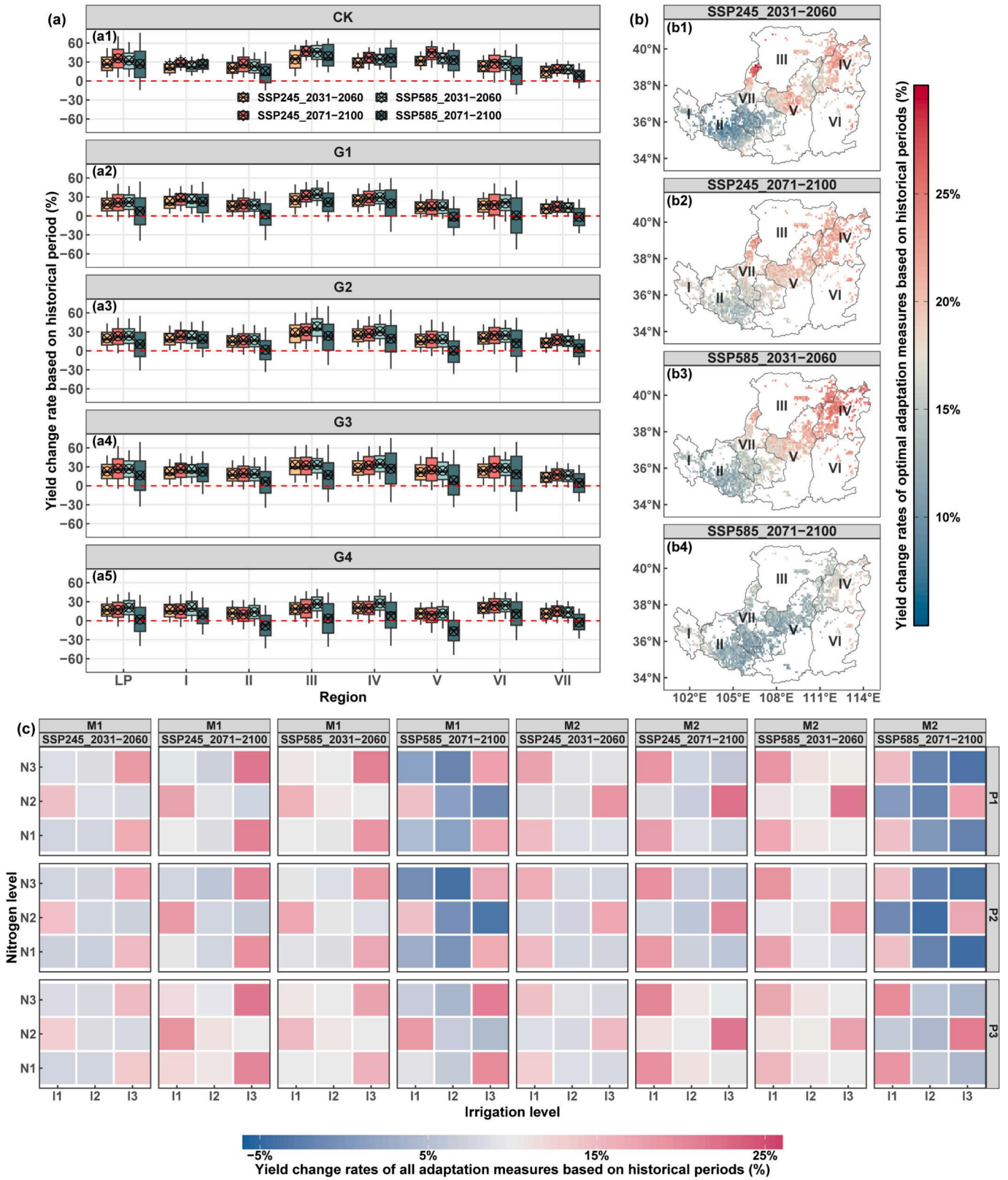


**Fig. 3.** Projected yield change rates of potatoes on the Loess Plateau of China for 2031-2060 and 2071-2100 under SSP245 and SSP585 scenarios, relative to the baseline. (a) Relative yield change rates for different groups. In each box plot, the box spans the 25$^{th}$ to 75$^{th}$ percentiles, the internal black line marks the median, and the cross-circle symbol indicates the mean values. The whiskers extend to the 10th and 90th percentiles. The red dashed line denotes the baseline. (b) Spatial distribution of yield change rates under the optimal adaptation measures for future periods. (c) Yield change rates of all adaptation combinations for 2031-2060 and 2071-2100 under the SSP245 and SSP585 scenarios, with each grid cell represent a specific combination. (For interpretation of the references to colour in this figure legend, the reader is referred to the web version of this article.)

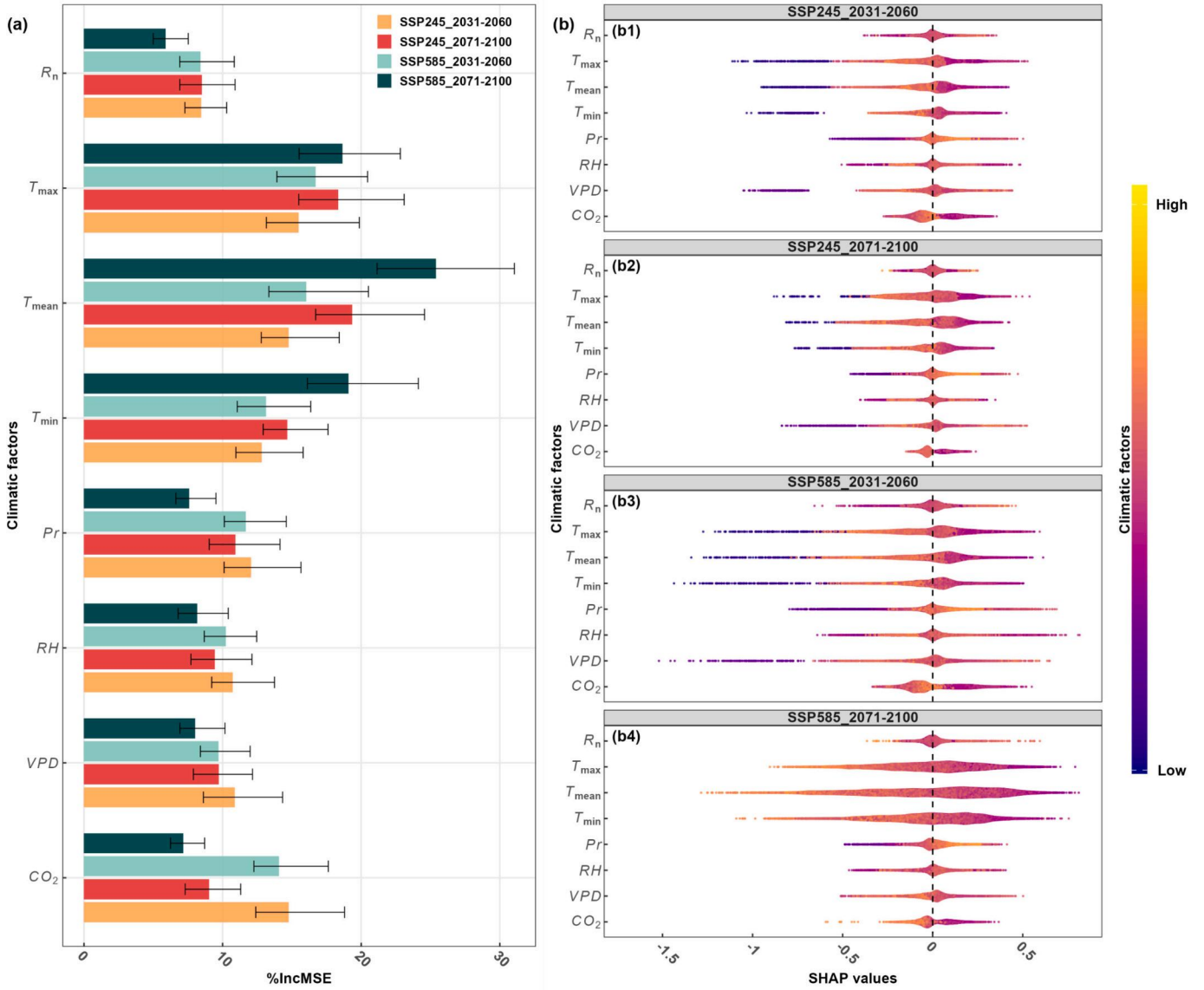


**Fig. 4.** Climatic drivers of potato yield on the Loess Plateau of China based on the random forest algorithm for 2031-2060 and 2071-2100 under SSP245 and SSP585 scenarios. (a) Relative importance of climatic factors affecting potato yield during the growing season (*Rn*: solar radiation, $T_{max}$: maximum temperature, $T_{min}$: minimum temperature, $T_{mean}$: mean temperature, *Pr*: precipitation, *RH*: relative humidity, *VPD*: vapor pressure deficit, $CO_2$: atmospheric $CO_2$ concentration). Error bars indicate the 95% confidence intervals, defined by the 5$^{th}$ and 95$^{th}$ percentiles from 1000 bootstrap samples. (b) Distribution of SHAP (Shapley Additive Explanations) values of climatic factors affecting potato yield.

20.78%, respectively. Among management practices, standardized yield increased with greater adaptation intensity for all measures except planting date (P). Irrigation (I) and plastic-film mulching (M) were the most effective measures for raising yield; however, under SSP585 their yield-enhancing effects fell by 45.00% and 18.75%, respectively, indicating that the potential of adaptation actions to increase yield diminishes under stronger climate change.

Spatially, *Pr* sensitivity was higher in the southwest and lower in the northeast, whereas the opposite pattern was observed for $T_{max}$: an effect that intensified under SSP585 (Table S9-S12). Coupling effects between climatic factors and adaptation measures were key drivers of yield outcomes. We identified significant antagonistic interactions between I and $CO_2$ and between I and $T_{max}$, though these antagonisms weakened under SSP585 (I-$CO_2$: -11.63%; I-$T_{max}$: -4.38%), suggesting that high $CO_2$ and high-temperature futures may reduce the marginal benefit of irrigation. Mulching (M) had opposite responses to high and low temperatures, which amplified the negative impacts of high temperature while mitigating low-temperature stress. *Pr* coupling positively with nitrogen (N) and showed a non-significant negative coupling with planting date (P), whereas $CO_2$ and N were negatively coupled. Most adaptation measures were negatively coupled with $T_{max}$, notably the P-$T_{max}$ coupling, underscoring the broad constraint imposed by high temperature on adaptation effectiveness. Furthermore, random effects in the model were identified: the year random effect increased over time in all regions, while the grid-cell random effect was higher but showed a declining trend in high-yield areas such as Gansu, Inner Mongolia, and northern Shanxi, particularly under SSP585. This may increase the uncertainty of the study in these regions (Fig. S16).

We decomposed contributions to yield change by factor type and found a consistent ranking under both SSP245 and SSP585: coupling factors > adaptation factors > climatic factors (Table S13). Overall, climatic factors, adaptation measures, and their coupling effects explained 65.47-88.04% of future potato yield variation. Under the SSP585 scenario, the contribution declined steadily during 2071-2100. Based on the standardized linear mixed model decomposition, coupling effects accounted for 37.63%-42.42% of future yield variation

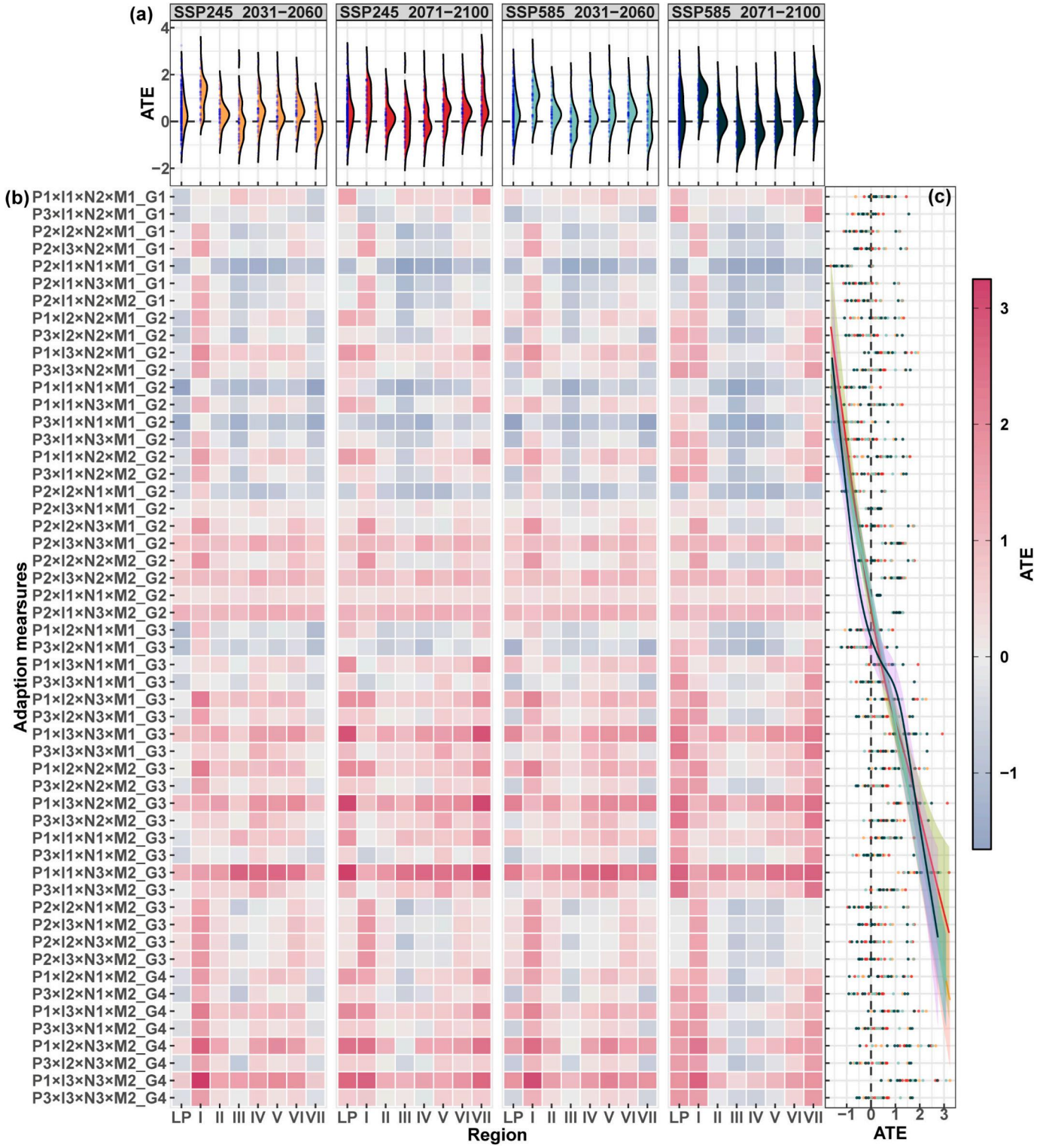


**Fig. 5.** Projected interannual variation in the Average Treatment Effect (ATE) of potato yield under different adaptation combinations, as driven by climatic factors across the Loess Plateau of China for 2031-2060 and 2071-2100 under SSP245 and SSP585 scenarios. (a) Distribution of ATE values across all 54 adaptation combinations, with the horizontal dashed line at ATE = 0 separating positive from negative treatment effects. (b) ATE values for individual adaptation combinations, ordered vertically from G1 (one measure adjusted) to G4 (all four measures adjusted). Within each group, combinations are sorted by increasing intensity of planting date adjustment, irrigation level, nitrogen rate, and mulching, illustrating how ATE changes as the number and intensity of measures increase. (c) Interannual ATE trajectories for each adaptation combination. Each solid curve represents one combination, with the shaded band denoting the 95% confidence interval derived from 1000 bootstrap replications within the MACF framework. Colors in all panels denote the period and emission scenario combination as indicated in the legend. All ATEs were estimated using the Multi-arm causal forest (MACF) model with 1000 bootstrap replications.

for the optimal combination. Across all adaptation groups, the coupling contribution of the highest-yielding combination was consistently greater than that of the lowest-yielding combination, highlighting substantial differences in how climate-adaptation coupling shape yield outcomes. Therefore, factors were further separated into positive (Fig. 7a) and negative (Fig. 7b) contributors. For the optimal adaptation combination, mean temperature ($T_{mean}$), *Pr*, and $CO_2$ were the main climatic drivers of yield increases (Table S14). $T_{max}$ was the sole climatic factor reducing yield, and under SSP585, it accounted for the largest share of yield loss among sub-factors (17.4%-25.9%). Because the optimal strategy was rainfed, irrigation contributed negatively to yield (SSP245: -19.3% to -16.8%; SSP585: -24.1% to -21.1%), although this negative effect eased over time, likely due to increased precipitation and mulching compensation.

Coupling effects dominated yield changes, especially in 2071-2100. Positive coupling pairs such as N-*Pr*, N-*VPD*, and M-*Pr* were the main drivers of yield increases. Couplings involving $T_{max}$ substantially reduced yields, with contributions that varied by period. Spatiotemporal analysis indicated that Qinghai, Gansu, and Ningxia benefited most from climate-adaptation coupling, although this benefit declined with higher emission intensity (Fig. S17-S21). Under SSP245, although the overall coupling effect weakens over time, the area where coupling increases yield by more than 40% expands markedly. In contrast, under SSP585, this area shows a clear shrinking trend (Fig. 7c). Therefore, we recommend shifting the emphasis of adaptation from water management alone toward heat stress mitigation and dynamic regional optimization. In the arid, cool west, modest wetting trends could be used to enhance synergies among water, fertilizer, and mulching. In the warmer, wetter east, strategies such as earlier planting should be used to avoid peak heat, and irrigation should be applied cautiously to prevent hot-wet coupling. Because marginal gains from stacking measures will continue to decline, adaptation design should prioritize combinations that maximize positive climate-management synergies rather than simply adding practices. This simulation derived regional priorities warrant further comprehensive evaluation that incorporates economic feasibility, water availability, and other practical constraints.

## 4. Discussion

### 4.1. Adaptive potential and limitations of potato yield on the loess plateau under climate change

By systematically evaluating multiple combinations of adaptation measures, this study identified the integrated strategy of early planting, rainfed management, increased nitrogen application, and plastic film mulching (P1×I1×N3×M2) as the most effective package for potato production on the Loess Plateau. This strategy increased future yield by 19.50%-20.94% (Fig. 2c), demonstrating that comprehensive management produces greater yield gains than any single measure under climate change (Abramoff et al., 2023). Notably, the yield of the optimal combination was 6.26%-6.78% higher than the best combination in Group 4 (P1×I3×N3×M2), which is fully irrigated compared with the optimal strategy. In addition, warming largely offsets the improvement in water use efficiency associated with elevated $CO_2$, further diminishing the marginal benefit of irrigation (Kaminski et al., 2014). As a result, under mulching and intensified heat stress, particularly under SSP585, may expose irrigated fields to more severe hot-wet coupling stress, negating the positive effects of both irrigation and elevated $CO_2$. Overall, although multi-measure strategies provide a higher yield ceiling than single adaptations, their effectiveness is constrained by future warming. The yield benefits of adaptation measures also showed clear dependence on emission pathways and declined over time. Under the high-warming SSP585 scenario, especially during 2071-2100, the effectiveness of many adaptation combinations dropped sharply, with

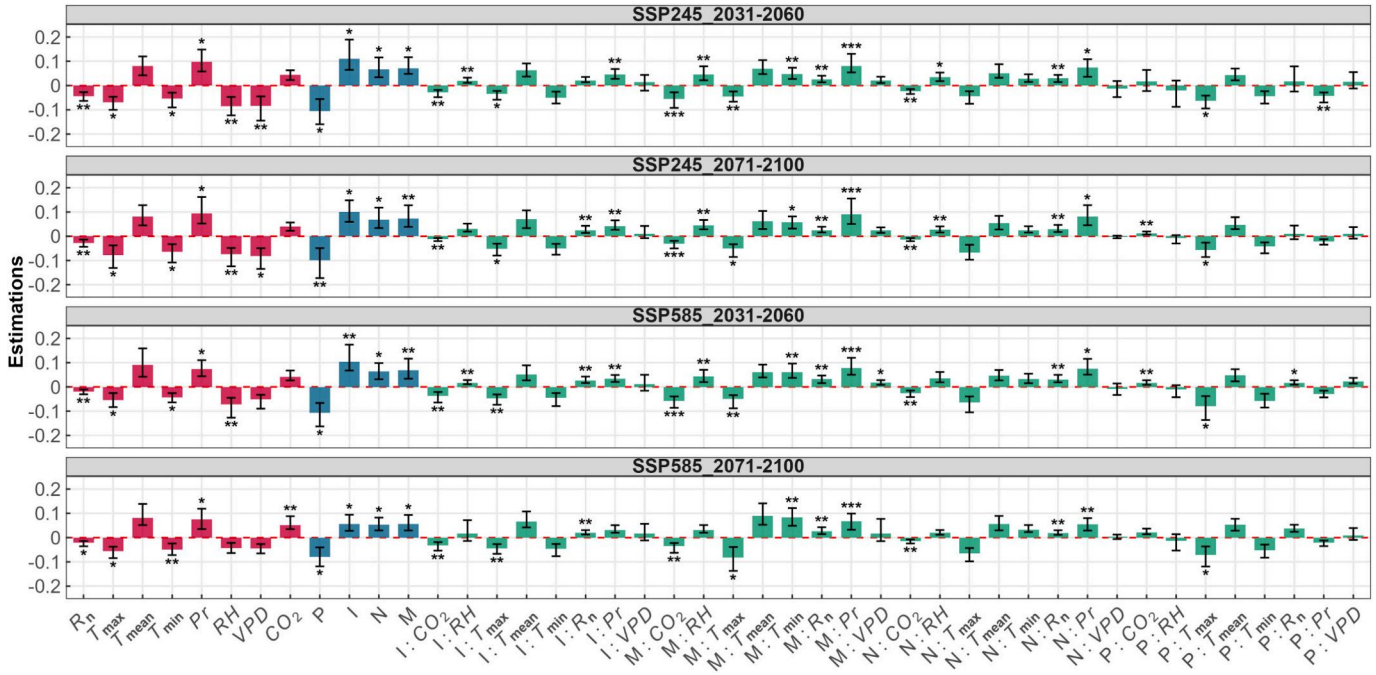


**Fig. 6.** Projected sensitivity of standardized potato yield to different types of factors across regions of the Loess Plateau in China during the 2031-2060 and 2071-2100 under SSP245 and SSP585 scenarios. Each panel corresponds to one period-scenario combination, with the seven regions arranged from left to right. Red bars represent climatic factors (*Rn*: solar radiation, $T_{max}$: maximum temperature, $T_{min}$: minimum temperature, $T_{mean}$: mean temperature, *Pr*: precipitation, *RH*: relative humidity, *VPD*: vapor pressure deficit, $CO_2$: atmospheric $CO_2$ concentration); blue bars represent adaptation measures (P: planting date, I: irrigation, N: nitrogen rate, M: mulching); and green bars represent climate-adaptation coupling terms. The height of each bar indicates the standardized sensitivity coefficient, with bars above zero denoting positive effects on yield and bars below zero denoting negative effects. Error bars show 95% confidence intervals from 1000 bootstrap replications. *, **, and *** denote $P < 0.05$, $P < 0.01$, and $P < 0.001$, respectively. (For interpretation of the references to colour in this figure legend, the reader is referred to the web version of this article.)

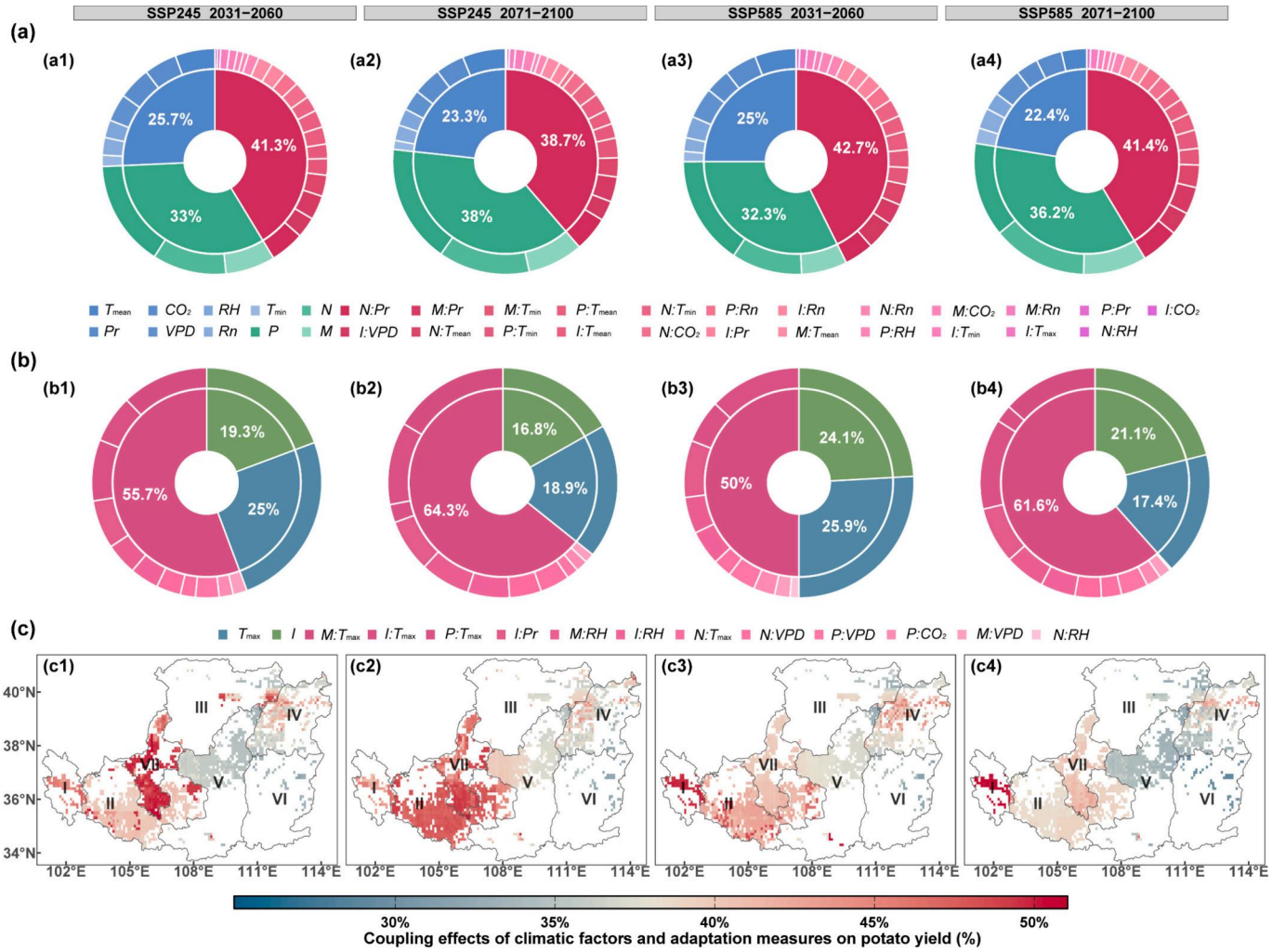


**Fig. 7.** Decomposition of contribution rates from different factor types to standardized potato yield under the highest-yielding adaptation combination (P1×I1×N3×M2: early planting, rainfed, 1.25 × local nitrogen rate, plastic mulching) during the 2031-2060 and 2071-2100 periods under SSP245 and SSP585 scenarios. (a) Proportion of individual factors among positive contributors to yield variation. Red colors denote climatic factors, blue colors denote adaptation measures, and green colors denote climate-adaptation coupling terms. The percentages are calculated from the LMM-based contribution decomposition. (b) Proportion of individual factors among negative contributors, with the same colour scheme. (c) Spatial distribution of the coupling contribution rate (%) across the Loess Plateau. Each grid cell is colored according to the percentage of yield variation explained by climate-adaptation coupling. Each column corresponds to one period-scenario combination. (For interpretation of the references to colour in this figure legend, the reader is referred to the web version of this article.)

several no longer improving yield (Fig. 3c). Kusmec and Schnable (2024) reported that adjusting planting dates alone is insufficient to offset the negative effects of projected warming, suggesting that climate change can strongly impair the performance of adaptive measures. As temperatures move beyond crop tolerance thresholds, the marginal returns of management practices decrease rapidly. The substantial increases in maximum and minimum temperatures observed in this study, along with intensified heat stress, likely undermine the benefits of irrigation and mulching (Fig. S2). These results highlight the need to incorporate the extremely and non-stationarity of future climate conditions when designing adaptation strategies (Minoli et al., 2022; Wescombe et al., 2025).

Our findings also show pronounced spatial variability in yield responses and adaptation benefits. Regions such as northern Shanxi achieved the highest yields under the optimal strategy, whereas Qinghai exhibited limited gains (Fig. 3b). This spatial pattern is closely linked to differences in climatic resources, water and nutrient availability (Rezaei et al., 2023). Consistent with previous modeling work on the Loess Plateau, the relatively warm and humid eastern regions benefit more from integrated strategies, while the arid and cool western regions face combined water and heat constraints (Zhang et al., 2024). Two mechanisms explain this pattern: first, differences in baseline resource limitations play a key role. Arid and cold regions respond strongly to water and soil management, where even moderate practices such as mulching or nitrogen application can substantially enhance yield potential (Zhang et al., 2025). Second, spatial variation in climate change is also important. Heat stress in the warmer eastern region can more readily offset the gains achieved through management practices. These results underscore the need for location-specific adaptation strategies: prioritizing water conservation and optimized nitrogen application under mulching in the arid-cold west, and focusing on heat mitigation in the east (e.g., adjusting planting dates, timely mulch removal, and reducing irrigation to avoid wet-heat coupling). Importantly, the original southwest to northeast yield gradient shifted under the SSP585 scenario (Fig. 3b), indicating that intensified climate change may reshape regional production patterns (Huang and Liu, 2025). Therefore, the selection of adaptation strategies must remain dynamic and context-dependent to safeguard future potato yield potential.

### 4.2. Causal drivers of potato yield under climate warming on the loess plateau

Building on the assessment of adaptation potential, we further examined the causal impacts and spatiotemporal patterns of climate-adaptation couplings using random forest and the multi-arm causal forest (MACF). During the historical period, $CO_2$ fertilization and precipitation were the primary drivers of yield variation. In future periods, however, the importance of temperature-related factors ($T_{max}$, $T_{min}$, and $T_{mean}$) increased sharply and became dominant, whereas the relative importance of $CO_2$ and precipitation declined (Fig. S9, 4a). This shift indicates that although $CO_2$ concentration and precipitation will continue to rise, their positive effects will be partly offset or even overtaken by the negative impacts of accelerated warming. Over the medium and long term, especially under high-emission scenarios, heat stress is therefore expected to replace water and $CO_2$ as the key climatic constraint on crop productivity (Hawkins et al., 2013). The SHAP values and their differences (SVD) provide a more detailed explanation for this transition. SHAP values for temperature factors increased at first but then declined as yield rose, especially under SSP585 (Fig. S12). This pattern reflects a nonlinear stress threshold effect: warming can promote growth within an optimal range, but once the threshold is exceeded, it leads to rapid yield loss. Increases in temperature within the moderate range may be partly offset by acclimation of photosynthesis and respiration, whereas sudden heatwaves or intense heat stress cannot be easily mitigated (Zhu et al., 2021). These interpretable machine-learning results complement traditional regression analyses by capturing complex nonlinear responses, thereby improving the reliability of the inferred mechanisms. Climatic drivers also showed marked east-west spatial differences. In the semi-arid western region (Qinghai, Gansu, Ningxia), the relative importance of water-related factors (*Pr*, *RH*, *VPD*) remained higher than that of temperature (Fig. S10). This reflects persistent water limitations in the region and supports the conclusion that the west is more responsive to water-conservation measures. By contrast, the more humid eastern region showed greater sensitivity to warming, suggesting that future adaptation strategies must be tailored to regional conditions (Pequeno et al., 2021).

Causal inference using the MACF model provides stronger evidence for the effect of climate-adaptation couplings. The optimal combination (P1×I1×N3×M2) produced the highest and most stable average treatment effect (ATE), confirming that its yield benefit arises from climatic drivers and adaptation responses rather than confounding factors (Fig. 5). Under SSP585 during 2071–2100, the second-best irrigation-based combination (P1×I3×N3×M2) exhibited a much larger yield loss, highlighting the higher risk and uncertainty of irrigation-dependent strategies under intense warming. Most adaptation combinations generated positive ATEs in the near-to-midterm, but their effectiveness declined over time and under higher emissions (Fig. 5c). Moreover, increasing the number of measures did not produce proportional gains; marginal benefits decreased gradually, indicating that adaptation planning should prioritize cost-effective combinations rather than simple accumulation of measures (Rurinda et al., 2015). In fact, the attenuation of ATE may be closely related to the nonlinear effects of temperature stress (Agnolucci et al., 2020). When temperatures continually exceed physiological thresholds, the resulting metabolic imbalances, such as inhibited photosynthesis and increased respiration, can weaken or override the positive physiological pathways enhanced by planting date adjustment, nitrogen application, or mulching (Medina and Tian, 2023). The spatial distribution of causal effects further shows that the western Loess Plateau had the highest concentration of positive ATEs, likely due to its lower current yield baseline and possible warm-wet seasonal improvements linked to slight wetting trends under climate warming (Fig. S13, S15). Ren et al. (2025) similarly found that integrated optimization of irrigation and nitrogen input is the most resource-efficient strategy for mitigating climate-driven yield losses in the United States, consistent with our findings. In summary, the spatiotemporal patterns revealed by the causal inference framework show that the yield-enhancing benefits of adaptation measures represent causal associations shaped by climatic stress thresholds within the simulated system. Their magnitude weakens systematically under future warming and is closely tied to the extent to which climatic change affects key physiological processes in the crop.

### 4.3. Mechanisms and uncertainties of coupling effects dominating future potato yield change

After identifying adaptation potential and the causal drivers of potato yield, we applied standardized linear mixed models to quantify the sensitivity and relative contributions of climatic factors, adaptation measures, and their interactions to future yield. Our results indicate that under sustained warming, crop physiological responses to water and nitrogen become downregulated, and the yield benefits of irrigation and plastic film mulching decline, particularly under high-emission scenarios (Fig. 6). This suggests that extreme heat in the future may modify or even reverse the effects of some conventional management practices. For example, although mulching can alleviate low-temperature stress, it may intensify yield losses under high-temperature and high-humidity conditions, consistent with previous studies (He et al., 2024; Tong et al., 2026). Within the optimal adaptation strategy, advancing the planting date was the most effective single measure, increasing future yield by 13.52% to 17.02% (Fig. 7a). Earlier planting allows potatoes to avoid the hottest part of the growing season, thereby reducing exposure to prolonged and intense heat, which was the only climatic factor showing a negative contribution to yield (Fig. 7b). The $CO_2$ fertilization effect also weakened, declining from 4.68% to 3.20%, likely because its benefits were increasingly offset by rising temperatures in later periods and under higher-emission scenarios, in agreement with observations from Europe and North America (Fleisher et al., 2021; Fleisher et al., 2017; Zhao et al., 2022). Interactions between climate and adaptation measures accounted for the largest share of yield variation, followed by adaptation measures alone and then individual climatic factors. Together, these components explained 65.5% to 88.0% of future potato yield change (Table S10). Climate-adaptation interactions therefore play a dominant role in shaping future yield patterns on the Loess Plateau (Fig. 7c). However, their contribution declined under higher-emission pathways and the distant future, indicating that the effectiveness of adaptation measures strongly depends on climate-mediated interactions within an evolving environmental background. For example, although irrigation (I) as an independent factor shows a negative contribution within the optimal combination, this highlights that the selected strategy avoids unfavorable interactions associated with increased irrigation while strengthening beneficial couplings (Fig. 7b). By adopting rainfed management (I1), it reduces the risk of humid and hot stress that irrigation may induce, while plastic film mulching (M) and increased nitrogen application (N) form strong positive synergies with changes in precipitation (*Pr*) and mean temperature ($T_{mean}$). According to the LMM-based contribution decomposition, coupling effects account for 37.63% to 42.42% of future yield variation (Table S10). This provides a key principle for designing dynamic climate-adaptive agricultural systems: integrated adaptation should not be a simple stacking of measures but a dynamic matching to shifting climatic conditions, aiming to maximize positive climate-adaptation synergies while avoiding detrimental interactions(Hultgren et al., 2025; Woo et al., 2022).

Although our research systematically reveals the response mechanisms and adaptation potential of potato yield under future climate change by integrating multi-model simulations, machine learning, and causal inference, the conclusions remain subject to uncertainties. First, the 27 GCMs used in this study exhibit differences in projected precipitation and temperature, which may introduce uncertainty into the estimated magnitude of yield changes (Jia et al., 2023). Second, the two crop models represent plastic film mulching in different ways. STICS simulates mulching mechanistically by accounting for radiation, heat,

and water barrier effects and dynamically coupling root growth with soil hydrothermal feedbacks, whereas AquaCrop uses an empirical approach based on an evaporation reduction coefficient and thermal time compensation. These multiple sources jointly contribute to uncertainty in the simulated yield responses (Asseng et al., 2013). As uncertainties may propagate and accumulate across the different stages of the analytical framework, the exact numerical estimates could be subject to some degree of bias. Nevertheless, the overall direction and spatial patterns of the findings are expected to remain robust and can still provide meaningful guidance for adaptation planning.

Despite these structural differences, the two models produced broadly consistent results in terms of interannual variation and the direction of yield responses to climate change across the 54 adaptation combinations. The main conclusions of this study are therefore not driven by the choice of a single model. Model performance may also be less reliable under extreme climatic conditions, which are difficult to represent accurately, even when long-term trends are captured. Furthermore, although the multi-arm causal forest (MACF) effectively captures nonlinearity and heterogeneity, the causal inferences rely on three key assumptions: that all relevant confounding variables have been measured and included, that each treatment has a non-zero probability of occurrence across the climate space, and that the simulated yield for a given management practice corresponds to what would be observed under that practice. These assumptions are generally met within our modeling framework, though unmeasured factors warrant caution in extrapolation. This limits the ability to attribute yield changes to factors beyond climate and management, such as soil degradation, pests, and diseases. Future studies should incorporate these processes to enable more precise and adaptive management under complex climate change. Quantifying the propagation of uncertainties across the full analytical chain also warrants further investigation. Overall, our findings highlight that ensuring food security in a warming climate requires close attention to the strong coupling between climate and adaptation measures to reduce risks to potato production.

## 5. Conclusion

We systematically evaluated potato production responses to future climate change on Loess Plateau of China. A comprehensive adaptation package combining early planting, rainfed management, increased nitrogen application, and plastic mulching (P1×I1×N3×M2) emerged as the highest-yielding strategy, increasing projected yields by 19.5-20.9% in the future. However, marginal benefits from adaptation measures exhibited diminishing returns and were substantially weakened under high-emission, long-term scenarios, indicating that ongoing warming will constrain their effectiveness. Using a multi-arm causal forest (MACF) model, we demonstrate through causal inference that climate-adaptation coupling significantly affects potato yield within the modeling framework. Furthermore, we found that adaptation packages relying on supplemental irrigation show a marked decline in causal effectiveness under intensified warming. This suggests that heat stress is likely to outweigh the positive effects of water and $CO_2$ fertilization and will become a primary causal constraint on potato production. Standardized linear mixed models showed that climate-adaptation couplings explained the largest share of yield variation, accounting for 37.63-42.42% of future yield changes. The optimal adaptation strengthened positive couplings such as nitrogen-precipitation (N-*Pr*) and mulching-precipitation (M-*Pr*), improving water-nutrient synergies under rainfed conditions while avoiding the compounded hot-wet stress that arise from irrigation combined with mulching under high temperatures. Spatiotemporal analysis indicated that the western Loess Plateau benefited most from climate-adaptation coupling, but these benefits were substantially reduced under the high-emission SSP585 scenario. In contrast, the eastern regions, being warmer and more humid, face greater heat stress and thus require distinct adaptation priorities, such as earlier planting and reduced irrigation to avoid compounded hot-wet stress. Consequently, adaptation planning must be regionally tailored to local climate intensity to stabilize food production.

Further work of the simulation priorities identified here should also incorporate field experiments, pest and disease dynamics, economic cost assessments, and water availability constraints, supported by long-term on-site validation to strengthen causal inference. In summary, under a non-stationary climate, dynamic, region-specific adaptation strategies grounded in climate-management coupling mechanisms are essential to maintain long-term stability and resilience of potato production on the Loess Plateau.

## CRediT authorship contribution statement

**Zhihao He:** Writing – review & editing, Writing – original draft, Software, Methodology, Formal analysis, Data curation, Conceptualization. **Tengcong Jiang:** Validation, Supervision, Methodology. **Lin Zhu:** Resources, Methodology, Data curation. **Ning Yao:** Supervision, Funding acquisition. **Yi Li:** Supervision. **Hao Feng:** Supervision, Funding acquisition. **De Li Liu:** Writing – review & editing, Supervision, Resources. **Liang He:** Resources, Methodology. **Jianqiang He:** Writing – review & editing, Supervision, Project administration, Funding acquisition. **Qiang Yu:** Writing – review & editing, Supervision, Resources, Funding acquisition.

## Declaration of competing interest

The authors declare that they have no known competing financial interests or personal relationships that could have appeared to influence the work reported in this paper.

## Acknowledgements

This research was partially supported by the National Natural Science Foundation of China (No. 52579046), the National Key Research and Development Program of China (2021YFD190070402), and Shaanxi Province “San-qin Scholars” innovation team Support Plan-Northwest A&F University Smart Agriculture Innovation Team.

## Appendix A. Supplementary data

Supplementary data to this article can be found online at https://doi.org/10.1016/j.agsy.2026.104848.

## Data availability

The historical meteorological data can be obtained at https://data.tpdc.ac.cn/en/data/e60dfd96-5fd8-493f-beae-e8e5d24dece4. The CMIP6 data can be accessed at https://esgf-node.llnl.gov/projects/cmip6/. The soil physicochemical properties can be accessed at https://www.fao.org/soils-portal/data-hub/soil-maps-and-databases/harmonized-world-soil-database-v20/ and http://globalchange.bnu.edu.cn. The STICS and AquaCrop emulators can be found at https://stics.inrae.fr/eng and https://www.fao.org/land-water/databases-and-software/aquacrop/. All data and code necessary to ensure the reproducibility of the results are available on the Zenodo website at https://zenodo.org/records/18195762; DOI: https://doi.org/10.5281/zenodo.18195762.

## References

Abramoff, R.Z., et al., 2023. Adaptation strategies strongly reduce the future impacts of climate change on simulated crop yields. Earth's Future 11 (4).
Agnolucci, P., et al., 2020. Impacts of rising temperatures and farm management practices on global yields of 18 crops. Nat. Food 1 (9), 562–571.
Asseng, S., et al., 2013. Uncertainty in simulating wheat yields under climate change. Nat. Clim. Chang. 3 (9), 827–832.
Breiman, L., 2001. Random forests. Mach. Learn. 45 (1), 5–32.

Brisson, N., Launay, M., Mary, B., Beaudoin, N., 2009. Conceptual Basis, Formalisations and Parameterization of the STICS Crop Model. Editions Quae.
Challinor, A.J., et al., 2014. A meta-analysis of crop yield under climate change and adaptation. Nat. Clim. Chang. 4 (4), 287–291.
Dobor, L., et al., 2016. Crop planting date matters: estimation methods and effect on future yields. Agric. For. Meteorol. 223, 103–115.
Fitzgerald, G.J., et al., 2016. Elevated atmospheric CO<sub>2</sub> can dramatically increase wheat yields in semi-arid environments and buffer against heat waves. Glob. Chang. Biol. 22 (6), 2269–2284.
Fleisher, D.H., et al., 2017. A potato model intercomparison across varying climates and productivity levels. Glob. Chang. Biol. 23 (3), 1258–1281.
Fleisher, D.H., et al., 2021. Yield response of an Ensemble of Potato Crop Models to elevated $CO_2$ in continental Europe. Eur. J. Agron. 126.
Fu, B., et al., 2017. Hydrogeomorphic ecosystem responses to natural and anthropogenic changes in the loess plateau of China. Annu. Rev. Earth Planet. Sci. 45 (1), 223–243.
Hawkins, E., et al., 2013. Increasing influence of heat stress on French maize yields from the 1960s to the 2030s. Glob. Chang. Biol. 19 (3), 937–947.
He, Z., et al., 2024. Clarifying the impacts of climatic coupling on plastic-mulching potato production in the loess plateau of China. Agric. Syst. 221, 104140.
Heinicke, S., Frieler, K.A., Jägermeyr, J., Mengel, M., 2022. Global gridded crop models underestimate yield responses to droughts and heatwaves. Environ. Res. Lett. 17 (4).
Huang, Y.H., Liu, Z.J., 2025. Increasing accumulated temperature pushed the maize planting limit northwards: phenomenon analysis and coping strategy. Earth's Future 13 (9).
Hultgren, A., et al., 2025. Impacts of climate change on global agriculture accounting for adaptation. Nature 642 (8068).
Jägermeyr, J., et al., 2021. Climate impacts on global agriculture emerge earlier in new generation of climate and crop models. Nat. Food 2 (11), 875.
Jia, Q.M., Jia, H.F., Li, Y.J., Yin, I.K., 2023. Applicability of CMIP5 and CMIP6 models in China: reproducibility of historical simulation and uncertainty of future projection. J. Clim. 36 (17), 5809–5824.
He Jie et al., 2025. China Meteorological Forcing Dataset v2.0 (1951–2024). In: C. National Tibetan Plateau Data (Editor). National Tibetan Plateau Data Center.
Kaminski, K.P., et al., 2014. Gas-exchange, water use efficiency and yield responses of elite potato (*Solanum tuberosum* L.) cultivars to changes in atmospheric carbon dioxide concentration, temperature and relative humidity. Agric. For. Meteorol. 187, 36–45.
Kim, H.Y., et al., 2003. Effects of free-air $CO_2$ enrichment and nitrogen supply on the yield of temperate paddy rice crops. Field Crop Res. 83 (3), 261–270.
Kluger, D.M., Owen, A.B., Lobell, D.B., 2022. Combining randomized field experiments with observational satellite data to assess the benefits of crop rotations on yields. Environ. Res. Lett. 17 (4).
Kusmec, A., Schnable, P.S., 2024. Phenological adaptation is insufficient to offset climate change-induced yield losses in US hybrid maize. Glob. Chang. Biol. 30 (10).
Li, Y., et al., 2020. Quantifying irrigation cooling benefits to maize yield in the US Midwest. Glob. Chang. Biol. 26 (5), 3065–3078.
Liu, B.B., et al., 2021. Promoting potato as staple food can reduce the carbon-land-water impacts of crops in China. Nat. Food 2 (8), 570–577.
Makowski, D., Marajo-Petitzon, E., Durand, J.L., Ben-Ari, T., 2020. Quantitative synthesis of temperature, $CO_2$, rainfall, and adaptation effects on global crop yields. Eur. J. Agron. 115.
McDermid, S., et al., 2023. Irrigation in the earth system. Nat. Rev. Earth Environ. 4 (7), 435–453.
Medina, H., Tian, D., 2023. Synergistic contributions of climate and management intensifications to maize yield trends from 1961 to 2017. Environ. Res. Lett. 18 (2).
Minoli, S., Jägermeyr, J., Asseng, S., Urfels, A., Müller, C., 2022. Global crop yields can be lifted by timely adaptation of growing periods to climate change. Nat. Commun. 13 (1).
Pequeno, D.N.L., et al., 2021. Climate impact and adaptation to heat and drought stress of regional and global wheat production. Environ. Res. Lett. 16 (5).
Raymundo, R., et al., 2018. Climate change impact on global potato production. Eur. J. Agron. 100, 87–98.
Ren, C.C., He, L.Y., Rosa, L., 2025. Integrated irrigation and nitrogen optimization is a resource-efficient adaptation strategy for US maize and soybean production. Nat. Food 6 (4).
Rezaei, E.E., et al., 2023. Climate change impacts on crop yields. Nat. Rev. Earth Environ. 4 (12), 831–846.
Rurinda, J., et al., 2015. Climate change and maize yield in southern Africa: what can farm management do? Glob. Chang. Biol. 21 (12), 4588–4601.
Schlenker, W., Roberts, M.J., 2009. Nonlinear temperature effects indicate severe damages to US crop yields under climate change. Proc. Natl. Acad. Sci. USA 106 (37), 15594–15598.
Steduto, P., Hsiao, T.C., Raes, D., Fereres, E., 2009. AquaCrop—the FAO crop model to simulate yield response to water: I. Concepts and underlying principles. Agron. J. 101 (3), 426–437.
Sun, W.Y., et al., 2016. Changes in extreme temperature and precipitation events in the Loess Plateau (China) during 1960-2013 under global warming. Atmos. Res. 168, 33–48.
Tong, X.Y., et al., 2026. More frequent precipitation during the maize growth period offsets the yield increasing effect of straw mulching in China: a meta-analysis. Soil Tillage Res. 256.
Wescombe, N.J., et al., 2025. It's time to consider global catastrophic food failures. Glob. Food Secur. 46.
Woo, D.K., Riley, W.J., Grant, R.F., Wu, Y.X., 2022. Site-specific field management adaptation is key to feeding the world in the 21st century. Agric. For. Meteorol. 327.
Yu, Q.Y., et al., 2020. A cultivated planet in 2010-part 2: the global gridded agricultural-production maps. Earth Syst. Sci. Data 12 (4), 3545–3572.
Zhang, L., et al., 2024. Plastic film mulching increases crop yields and reduces global warming potential under future climate change. Agric. For. Meteorol. 349.
Zhang, H.H., et al., 2025. Assessing the impact of extreme climate events on European gross primary production. Agric. For. Meteorol. 362.
Zhao, C., et al., 2017. Temperature increase reduces global yields of major crops in four independent estimates. Proc. Natl. Acad. Sci. USA 114 (35), 9326–9331.
Zhao, C., et al., 2022. Potential benefits of climate change for potatoes in the United States. Environ. Res. Lett. 17 (10).
Zhu, T.T., De Lima, C.F.F., De Smet, I., 2021. The heat is on: how crop growth, development, and yield respond to high temperature. J. Exp. Bot. 72 (21), 7359–7373.